

# A high-efficient triboelectric-electromagnetic hybrid nanogenerator for vibration energy harvesting and wireless monitoring

Jian HE<sup>1</sup>, Xueming FAN<sup>1</sup>, Dongyang ZHAO<sup>2</sup>, Min CUI<sup>1</sup>, Bing HAN<sup>3</sup>,  
Xiaojuan HOU<sup>1</sup> & Xiujian CHOU<sup>1\*</sup>

<sup>1</sup>*Science and Technology on Electronic Test and Measurement Laboratory, North University of China, Taiyuan 030051, China;*

<sup>2</sup>*Beijing Institute of Computer Application, China North Industries Group Corporation Limited, Beijing 100089, China;*

<sup>3</sup>*College of Mechatronic Engineering, North University of China, Taiyuan 030051, China*

Received 25 June 2020/Revised 23 August 2020/Accepted 18 September 2020/Published online 23 August 2021

**Abstract** Scavenging mechanical vibration energy by combining triboelectric nanogenerators (TENGs) and electromagnetic generators (EMGs) is a renewable and low-carbon way to generate electric power. In this paper, we fabricate a cylindrical structure hybrid nanogenerator based on spring structure to effectively scavenge vibration energy. The introduction of spring structure not only enhances the space utilization, but also supports the moving magnet. Owing to its innovative structure, the instantaneous output power of TENG and EMG are 0.88 mW at a load of 10 M $\Omega$  and 216.7 mW at a load of 60  $\Omega$ , respectively. With the aids of a power management circuit, the hybrid nanogenerator can provide continuous power for two hygrometers connected in series. In addition, a self-powered wireless acceleration sensing monitoring system (SWAM) is developed to measure the acceleration signals of vibration sources. This study provides a novel guideline for harvesting mechanical vibration energy.

**Keywords** mechanical vibration energy, spring structure, triboelectric, electromagnetic, wireless monitoring system

**Citation** He J, Fan X M, Zhao D Y, et al. A high-efficient triboelectric-electromagnetic hybrid nanogenerator for vibration energy harvesting and wireless monitoring. *Sci China Inf Sci*, 2022, 65(4): 142401, <https://doi.org/10.1007/s11432-020-3081-4>

## 1 Introduction

Nowadays, with the development of sensor technology and low power devices, more and more new products such as mobile terminals, portable electronics and wireless sensors are changing our daily lifestyle [1]. The emergence of these electronic devices accelerates the transmission of information, and brings great convenience. The power supply is a problem in the information and intelligence era. At present, the power supply mostly depends on batteries [2]. However, tens of billions of batteries are abandoned every year because of the short service life and other shortcomings [3–6]. These abandoned batteries contain a variety of heavy metal elements and cause irreversible pollution to the environment. Accordingly, it is necessary to develop a renewable and low-carbon energy resource for adopting the development of the information era.

In the real world, mechanical vibration energy is distributed widely. To power new products, considerable efforts have been devoted to converting mechanical vibration energy to electricity, such as electromagnetic [7], piezoelectric [8–10] and triboelectric mechanisms [11–16]. Among the three energy transduction mechanisms, electromagnetic and triboelectric mechanisms have been used widely for their high output performance and simple structure. Especially, as a new type of vibration energy harvesting

\* Corresponding author (email: [chouxiujian@nuc.edu.cn](mailto:chouxiujian@nuc.edu.cn))

device, triboelectric nanogenerator (TENG) has attracted more and more attention in the field of self-powered supply for its advantageous properties, such as green environmental protection, light weight, high energy conversion efficiency, and low cost [17–19]. The output power of generator by a single energy conversion mechanism has been improved with the optimization of the material and device structure in recent decades [20–22]. However, the low energy harvesting efficiency still impedes its extensive application in daily life. By integrating various energy harvesting transduction mechanisms, the energy conversion efficiency is improved. Therefore, many hybrid nanogenerators have been designed to meet the power needs of some electronics [23–27]. At present, most power generation units of hybrid energy harvester consist of TENG, piezoelectric nanogenerator (PENG) and electromagnetic generator (EMG). As TENG and EMG have a good response to low frequency excitation and high frequency excitation respectively, the combination of TENG and EMG can not only improve the output performance of the device, but also broaden the working frequency band.

Herein, we present a triboelectric-electromagnetic hybrid nanogenerator based on two parallel spring structures (PS-HNG) to capture more mechanical energy through the supplemental conversion mechanism. The device shell and spring structure of PS-HNG are manufactured by 3D printing technology with acrylonitrile butadiene styrene copolymers (ABS) and Nylon materials, respectively. The fabricated device is characterized by a dimension of  $\Phi 70$  mm  $\times$  50 mm and a weight of 404 g. The maximum output power of TENG and EMG are 0.88 mW at a load of 10 M $\Omega$  and 216.7 mW at a load of 60  $\Omega$ , respectively. The bottom triboelectric nanogenerator (B-TENG) and bottom electromagnetic generator (B-EMG) can simultaneously light up 75 light emitting diodes (LEDs) connected in series and 189 LEDs connected in parallel, and the PS-HNG can power two hygrometers. In addition, a self-powered wireless acceleration sensing monitoring system (SWAM) is fabricated to measure the acceleration of vibration source. The result demonstrates that the hybrid nanogenerator provides an effective approach to capture the ambient energy.

## 2 Experimental section

**Fabrication of hybrid nanogenerator:** The room temperature vulcanized silicone rubber (RTV) was selected as the material of negative triboelectric film. The preparation of silicone film was completed in two steps. Firstly, the RTV and curing agent were mixed uniformly with a ratio of 100:2. Secondly, after being distributed well, the silicone was evenly coated on a smooth acrylic plate by using an applicator with a prefabricated height of 1 mm, and then placed at room temperature for 12 h. The obtained silicone film and conductive fabric were cut into a circle with the same diameter as the spring structure by using a cutting tool and then adhered to one side of the spring structure. The positive triboelectric film (conductive fabric) was adhered to another side of the spring structure in the same way. The EMGs were composed of two coils and a cylindrical permanent magnet. The turns of coil were set to approximately 600 and the wire diameter was 0.2 mm. The circular NdFeB magnet with a diameter of 60 mm was placed between the two spring bodies. The spring structures and the shell were produced by 3D print technology.

**Measurement system:** The output characters of TENGs and EMGs were detected by a programmable electrometer (Keithley 6514 System Electrometer) and a digital sourcemeter (Keithley 2611B). The lab-vibration system was composed of an arbitrary function generator (GWINSTEK, AFG-2225), power amplifier (SINOCERA, YE5872A), and electro-dynamics vibration generator (JZQ-200). The acceleration value of the hybrid nanogenerator was recorded by an impedance head (IEPE, 504AF02) which was installed on the electro-dynamics vibration generator.

## 3 Results and discussion

### 3.1 Device structure

The assembly process of the hybrid nanogenerator is illustrated in Figure 1(a). The hybrid nanogenerator is structurally symmetrical between top and bottom. It consists of two EMGs and two TENGs. A circular NdFeB permanent magnet (diameter of 60 mm and height of 9.5 mm) is placed in the middle of the upper and lower spring structures. The top electromagnetic generator (T-EMG) and B-EMG are formed by the circular magnet and two coils wrapped around the cylindrical structure. TENG is composed of

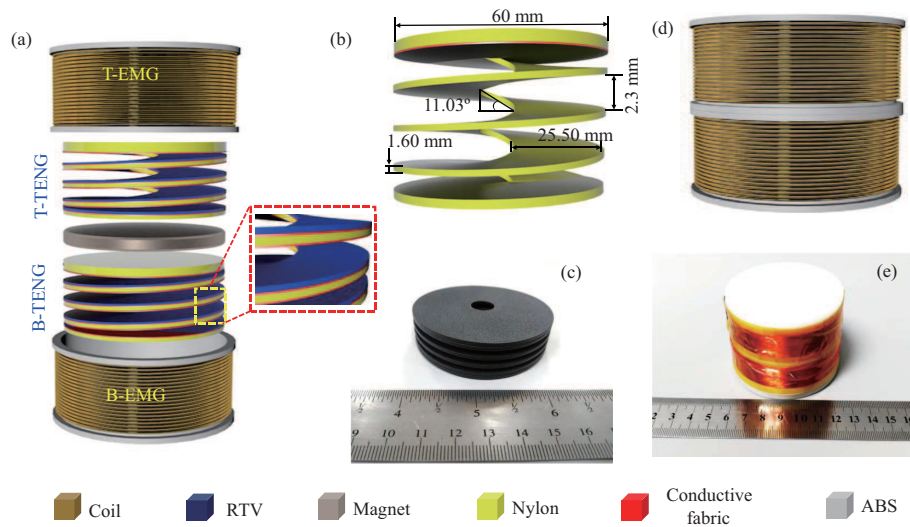


**Figure 1** (Color online) Schematic diagram of the designed triboelectric-electromagnetic hybrid nanogenerator. (a) The exploded diagram of energy harvester structure; (b) the size of spring structure; (c) the photo of spring structure; (d) 3D schematic of the hybrid nanogenerator; (e) the photo of device structure.

conductive fabric and RTV covered with conductive fabric. Silicone is a kind of negative material with strong electronic ability, and conductive fabric works as positive friction material and electrode at the same time. Positive material and negative material are respectively attached to the opposite side of the spring structure. The outside diameter, rotation layer width, rotation layer thickness, layer spacing, and helix angle are 60 mm, 25.5 mm, 1.6 mm, 2.3 mm and  $11.03^\circ$ , respectively (Figure 1(b)). The spring structure is manufactured by 3D printing technology using high-strength Nylon materials (Figure 1(c)). Owing to the spiral structure, TENG can be pressed and released without any other elastic support, and the area of friction layers can be increased in a limited volume. Two spring structures with frictional materials and a circular magnet are encapsulated in cylindrical structures (Figures 1(d) and (e)). The whole device has a small dimension of 70 mm×50 mm and a light weight of 404 g.

### 3.2 Working principles

The working principles of EMG and TENG are shown in Figures 2(a) and (b), respectively. When the device is in a static state, the circular magnet is completely outside of the top coils and bottom coil as the spring force at the bottom, and the flux through the coil remains constant. When the device is subjected to vibration excitations, owing to the effect of inertia, the magnet will move relative to the device, and the flux through the coils will change, thereby generating an induced current in both coils. The current generated in two coils is opposite polarity output. The working principle of TENG is based on triboelectric effect and electrostatic induction. When two friction materials (conductive fabric and silicone) with different polarities are in contact (state I), the surface of conductive fabric is positively charged and the surface of silicone is negatively charged. Owing to the insulation of the polymeric material, these surface charges can be maintained for a certain period of time [28]. As the separation distance between conductive fabric and silicone layer increases (state II), the electrons on the electrode of silicone layer gradually flow to conductive fabric. Until the spring structure is fully released (state III), a new potential balance is formed between silicone layer and its electrode without current flowing. Subsequently, with the external force applied to the spring structure increasing again, the spring structure is compressed again (state IV), resulting in the decrease of the distance between the two friction materials. The electrons on the conductive fabric gradually flow to the silicone electrode layer until two friction materials completely contact to form a new potential balance. After that, a full cycle of a electricity generation process is completed and another cycle begins. In order to further describe the potential distribution of TENG, the finite element method is used to analyze the process under open-circuit conditions (Figure 2(c)). When the two friction materials are in complete contact, the surface potential difference is zero. It can be seen that as the separation distance between the two friction materials increases, the surface potential difference gradually increases.

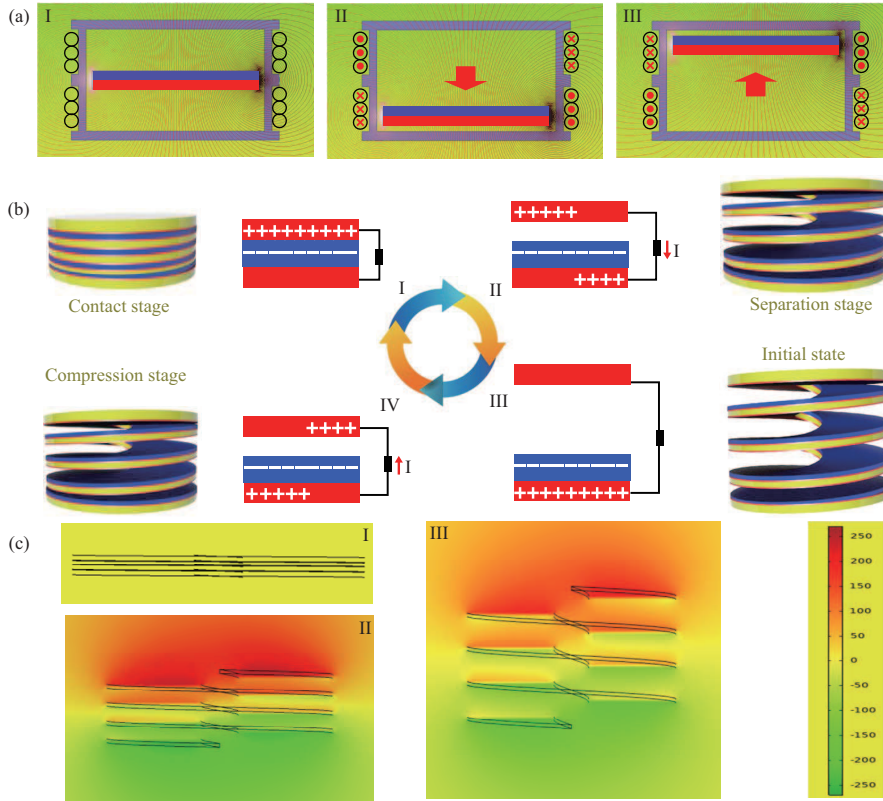


**Figure 2** (Color online) The working principles of (a) EMGs and (b) TENG. (c) The simulation analysis of potential distribution between the electrodes of TENG.

### 3.3 Dynamical response analysis

In practical application, owing to the influence of the size, density, hardness and other factors of obstacles, the vibration sources such as hydraulic breaker need to produce different levels of acceleration for crushing operation. Therefore, it is necessary to measure the output performance of devices under different accelerations. Figure 3 shows the electrical output performance of TENGs under different accelerations at a constant frequency of 3 Hz. The output performance of two energy-conversion mechanisms was measured under the different accelerations. As the acceleration increases linearly from 3 to 6 m/s<sup>2</sup>, the open-circuit voltage ( $V_{oc}$ ) of Top-TENG (T-TENG) increase from 10.56 to 41.84 V (Figure 3(a)), and short-circuit current ( $I_{sc}$ ) of T-TENG ranges from 0.60 to 1.87  $\mu$ A (Figure 3(b)). The  $V_{oc}$  of B-TENG is from 153 to 252 V, and the value of  $I_{sc}$  increases from 8.69 to 16.7  $\mu$ A. That is because that the force exerted by the circular magnet on the spring structure is gradually increasing with the increase of acceleration. The increase of interaction force leads to more sufficient material surface contact for two types of friction materials [29]. As depicted in Figures 3(c) and (f), the output voltages of T-TENG and B-TENG increase with the increase of external resistance, especially after the loading resistance of 10 M $\Omega$ . The maximum output powers of T-TENG and B-TENG are 15.4  $\mu$ W and 883.6  $\mu$ W at a loading resistance of 10 M $\Omega$ , respectively. The power calculation formula is  $P = U^2/R$ , where  $U$  is the output voltage and  $R$  is the loading resistance. The amplitude acceleration and frequency in the power test are 6 m/s<sup>2</sup> and 3 Hz, respectively. It should be noted that the output performance of T-TENG is lower than that of B-TENG. The difference is attributed to the effect of magnet gravity on the spring structures. For B-TENG, the gravity of the magnet and the external force on the device are superimposed to increase the contact force of the B-TENG friction layers, making the friction layers contact more fully with each other. Whereas for the T-TENG, the contact force is decreased because the gravity does negative work.

Subsequently, the influences of vibration acceleration on the output performance of EMGs are investigated. For EMG units, the output performance under different accelerations has a similar trend as TENG units. The output voltage, current, and output power for EMGs are shown in Figures 4(a)–(f). With the increase of acceleration from 3 to 6 m/s<sup>2</sup>,  $V_{oc}$  and  $I_{sc}$  of B-EMG increase from 4.49 to 9.31 V and from 38.6 to 98.4 mA, respectively. The output characteristic of T-EMG is similar to that of B-EMG. As

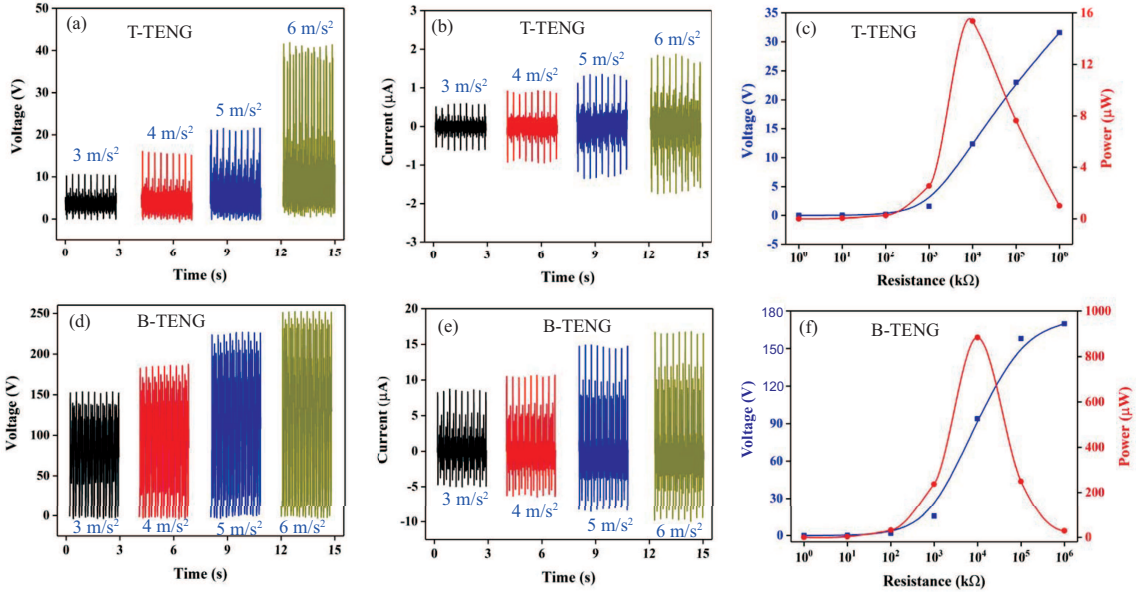


**Figure 3** (Color online) (a) and (b) Voltage and current signals of T-TENG at different acceleration. (c) Output power of T-TENG at the acceleration of  $6 \text{ m/s}^2$ . (d) and (e) Voltage and current signals of B-TENG at different acceleration. (f) Output power of B-TENG at the acceleration of  $6 \text{ m/s}^2$ .

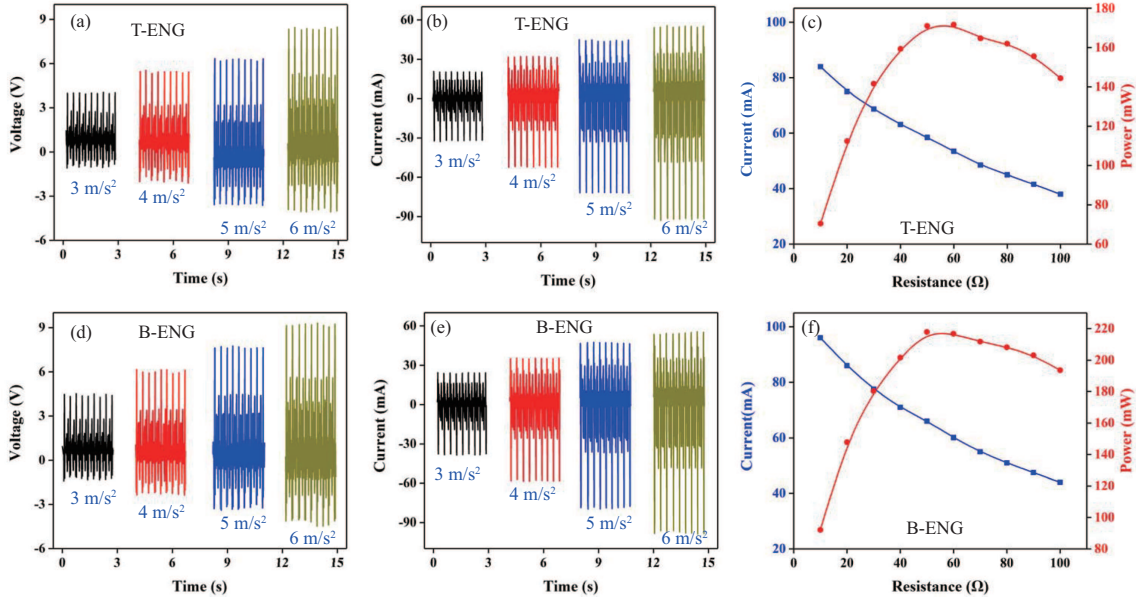


**Figure 4** (Color online) (a) and (b) Voltage and current signals of T-EMG at different acceleration. (c) Output power of T-EMG at the acceleration of  $6 \text{ m/s}^2$ . (d) and (e) Voltage and current signals of B-EMG at different acceleration. (f) Output power of B-EMG at the acceleration of  $6 \text{ m/s}^2$ .

shown in Figures 4(c) and (f), the maximum output powers of T-EMG and B-EMG are  $171.7 \text{ mW}$  and  $216.7 \text{ mW}$  at an external load resistance of  $60 \Omega$ . The power calculation formula is  $P = I^2 R$ , where  $I$  represents the current. The results are consistent with Faraday's law, in which the  $V_{oc}$  of EMG is related to the velocity between magnet and coil and is given as follows [30]:

$$V_{oc} = -NS \frac{dB(x)}{dt} = -NS \frac{dB(x)}{dx} \frac{dx}{dt} = -NS \frac{dB(x)}{dx} v, \quad (1)$$

where  $N$  and  $S$  are the turns and the area of the coil,  $B(x)$  is the magnetic flux density through the coil, and  $v$  is the velocity of the magnet.  $I_{sc}$  generated in the coils can be expressed as

$$I_{sc} = \frac{V_{oc}}{R_{coil}} = -\frac{NS}{R_{coil}} \frac{dB(x)}{dx} v, \quad (2)$$

where  $R_{\text{coil}}$  is the internal resistance of the coil. It should be noted that the output performance of EMGs is also affected by magnet gravity. However, the effect is much smaller than that of TENGs. The output performance of TENG is related to the contact area between the two friction surfaces, which can be affected by an external force to some extent. In contrast, the output performance of EMG is related to the change of magnetic flux, which is a kind of ultra-distance. Therefore, TENG is more sensitive to the change of external force.

As the energy harvesting units consist of two parallel springs and one circular magnet. When the magnet is excited by the external force once, the magnet will vibrate up and down many times. Figure S1 shows the output performance of T-TENG and B-EMG at an external excitation frequency of 3 Hz. It can be seen that both B-TENG and B-EMG can generate six electrical signal peaks in one cycle. The first peak is larger than the others, which is produced by external excitation, while other peaks originate from the spring rebound. The reliability and durability of the PS-HNG play an important role in whether it can be applied in practice application. In the follow-up experiment, the four generation units are tested (T-TENG, B-TENG, T-EMG, B-EMG) for a long-term operation. As shown in Figure S2, the output current of EMGs and TENGs does not change significantly after an operation of 1200 s. the reliability and durability test results show the great mechanical stability and reliability of the PS-HNG in a long-term operation.

### 3.4 Device application

Since both TENGs and EMGs generate alternating current (AC) signals, it is necessary to use full-wave rectifying bridges to convert AC signals into direct current (DC) signals and store in an energy storage device such as a capacitor or battery. Figure 5(a) shows the charging curves of individual generators charging a capacitor of 100  $\mu\text{F}$  at the acceleration of 6  $\text{m/s}^2$ . The charging curves indicate the advantages of the hybrid nanogenerator over the individual energy harvesting unit (B-TENG, B-EMG, and B-EMG//B-TENG). The charging characteristics are the external representation of the inherent output performance of the generators. The charging speed is determined by the generated current, and the final charging voltage of the capacitor is determined by the generated voltage. According to the results, owing to the high current and low voltage output of EMG, the capacitor can be charged to a stable voltage in a short time. However, the charging result of TENG is in contrast to that of EMG. By integrating TENG and EMG units, the capacitor can get a high charging voltage. As the capacitor is charged, it can be worked as an energy bank to power electrical products. In Figure 5(b) and Movie 1, two hygrothermographs connected in series are powered by a capacitor of 1000  $\mu\text{F}$  under an acceleration of 6  $\text{m/s}^2$ . The PS-HNG can provide continuous electric energy for the hygrothermographs after the capacitor is stored. Subsequently, Then, in order to characterize the actual power output effect of each power generation unit, the B-TENG and B-EMG are chosen to light up 75 LEDs connected in series and 189 LEDs connected in parallel after a rectified bridge (Figures 5(c) and (d), Movie 2). It can be seen from Movie 2 and Figure 5 that the brightness of LEDs lighted by B-EMG is much brighter than that of TENG. That is because the output current of EMG is much larger than that of TENG.

Furthermore, to monitor the dynamical response such as the acceleration of hydraulic breaker, a self-powered wireless acceleration sensing monitoring system (SWAM system) is developed. The system is composed of energy harvesting units, a power management circuit, and a 9-axis bluetooth attitude sensor (Figures 6(a) and (b)). During the test period, to reduce the influence of the electrodynamic vibration generator on the magnet of PS-HNG, a transition body ( $\Phi 70 \text{ mm} \times 90 \text{ mm}$ ) is installed between PS-HNG and electrodynamic vibration generator. The power management circuit includes rectified bridges and an energy storage unit (4700  $\mu\text{F}$  capacitor). The 9-axis bluetooth attitude sensor consists of bluetooth antenna, RF chip (nRF52832), highly integrated sensor chip (MPU9250), and power chip. The 9-axis bluetooth attitude sensor needs no more than 16 mA during active mode and no more than 0.1 mA during sleep mode according to the instruction. The working current of the 9-axis bluetooth attitude sensor is 14 mA which is measured by us with a DC regulated power supply (UNI-T, UTP3313TFL). The capacitor of 4700  $\mu\text{F}$  is charged to 5.7 V by the PS-HNG in 5 s at an acceleration of 8  $\text{m/s}^2$ , as shown in Figure 6(c). As observed in the voltage curve of the capacitor, after the SWAM system is connected to the circuit, the voltage of the capacitor decreases for a short time and then rises again. When the SWAM system is matched with a smart phone, the internal voltage of the capacitor stabilizes at about 2 V. With the continuous operation of SWAM system (as shown in Movie 3), the acceleration signals are transmitted to a smart phone via the bluetooth antenna and the signal curves are displayed in the

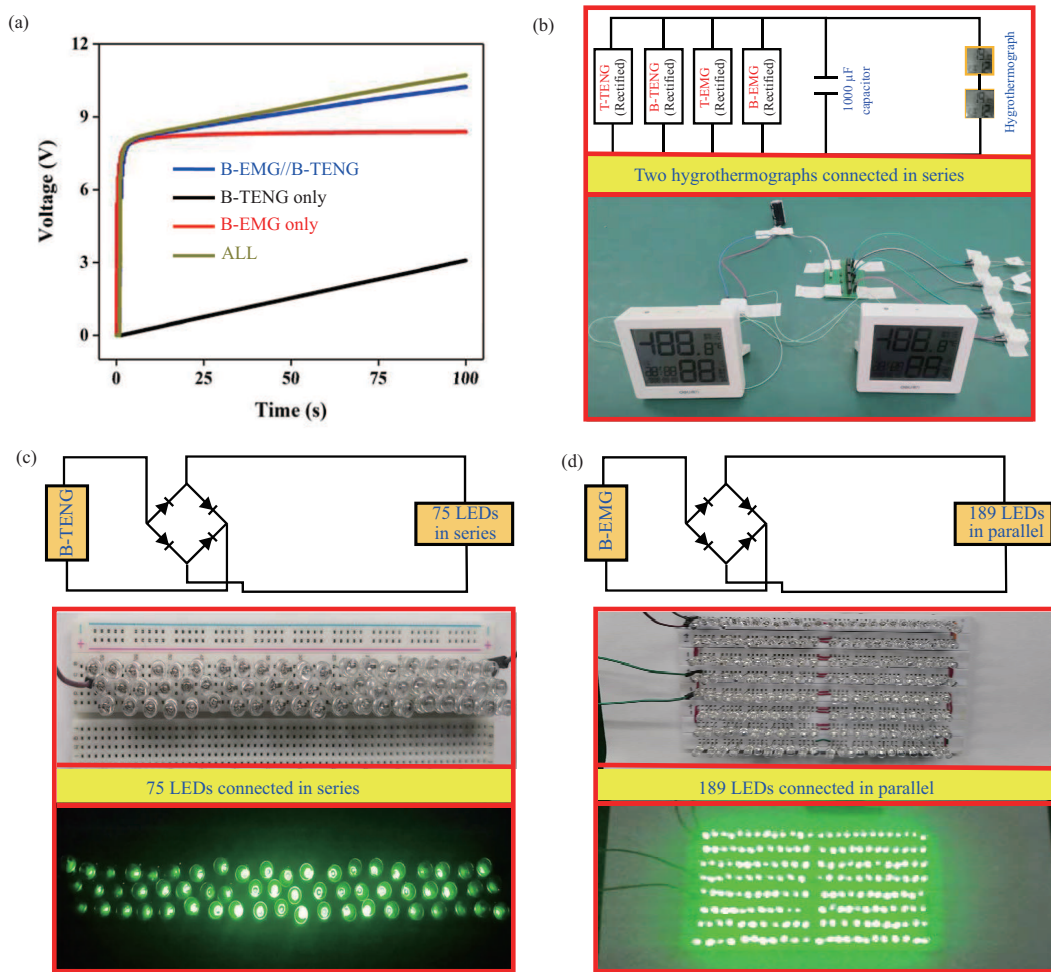


**Figure 5** (Color online) (a) Charging curves of a 100  $\mu\text{F}$  capacitor by the device at the acceleration of  $6 \text{ m/s}^2$ . (b) Powered by the hybrid nanogenerator for two hygrothermographs connected in series. (c) Photograph of 75 LEDs lighted by B-TENG after rectification. (d) Photograph of 189 LEDs lighted by B-EMG after rectification.

monitoring interfaces (Figure 6(d)). This work shows that the hybrid nanogenerator proposed by us has a potential application prospect in the self-powered acceleration monitoring system.

As the PS-HNG is fully packed by ABS sheet except for coils, the hybrid nanogenerator is isolated from the ambient environment. Consequently, the high humidity environment cannot affect the output performance of the hybrid nanogenerator. Thanks to its portability (small volume and light weight), the PS-HNG can be installed on the vibration equipment without any drastic changes in the facilities. Besides, the device has the characteristics of low cost and high performance, which make it possible to have a premise of widespread promotion. Most importantly, the innovative structure can not only be used to capture the vibration mechanical energy of large-scale facilities, but also to harvest the mechanical energy of human motion, and to provide supplemental electric energy for field operators.

## 4 Conclusion

In summary, we have presented a self-powered portable triboelectric-electromagnetic hybrid nanogenerator for vibration mechanical energy harvesting. The device is an enclosed cylindrical structure with a dimension of  $\Phi 70 \text{ mm} \times 50 \text{ mm}$  and a weight of 404 g. The device is a combination of TENGs and EMGs. The core of the proposed device is the spiral structure, which carries TENG friction layers and supports the magnet. Two coils wrapped on the shell are designed to harvest the vibration energy of the magnet converting it into electrical energy output. The results indicated that the hybrid nanogenerator can efficiently obtain energy at different accelerations. The instantaneous output power of TENG and

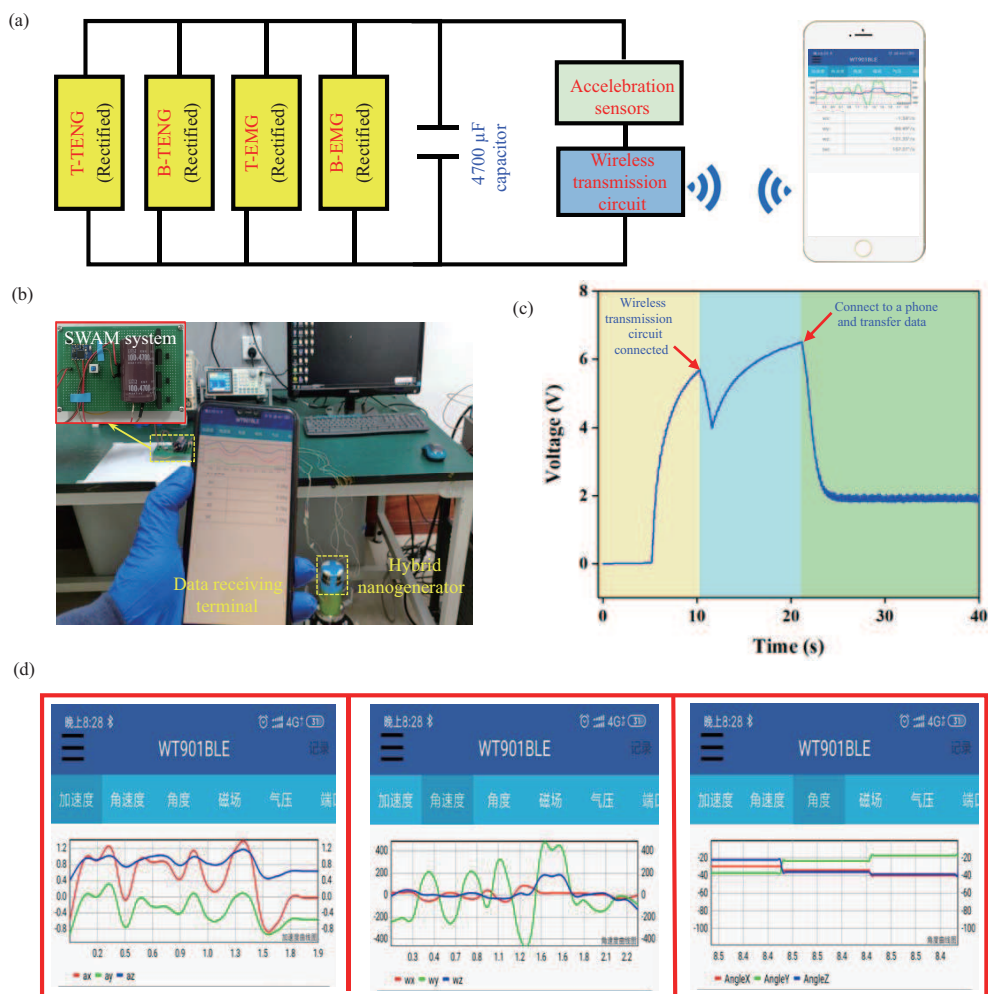


**Figure 6** (Color online) (a) The schematic circuit diagram of the self-powered wireless acceleration sensor system; (b) circuit diagram of self-powered wireless acceleration system powered by the PS-HNG; (c) the voltage of 4700  $\mu\text{F}$  capacitor used as a storage bank and power unit for SWAM system; (d) received different acceleration curves in the monitoring interface.

EMG are 0.88 mW at a load of 10  $\text{M}\Omega$  and 216.7 mW at a load of 60  $\Omega$ , respectively. The B-TENG and B-EMG can light up 75 LEDs connected in series and 189 LEDs connected in parallel, respectively. Two hygrothermographs connected in series can be powered by the PS-HNG through a power management unit. Moreover, a self-powered wireless acceleration sensor monitoring system is fabricated, which shows broad potential applications in all aspects of production and life.

**Acknowledgements** This work was supported by National Key R&D Program of China (Grant Nos. 2019YFF0301802, 2019YFB-2004802, 2018YFF0300605), National Natural Science Foundation of China (Grant Nos. 51975541, 51975542), Applied Fundamental Research Program of Shanxi Province (Grant No. 201901D211281), Program for the Innovative Talents of Higher Education Institutions of Shanxi.

**Supporting information** Figures S1 and S2. The supporting information is available online at [info.scichina.com](http://info.scichina.com) and [link.springer.com](http://link.springer.com). The supporting materials are published as submitted, without typesetting or editing. The responsibility for scientific accuracy and content remains entirely with the authors.

**References**

- 1 He J, Wen T, Qian S, et al. Triboelectric-piezoelectric-electromagnetic hybrid nanogenerator for high-efficient vibration energy harvesting and self-powered wireless monitoring system. *Nano Energy*, 2018, 43: 326–339
- 2 Rahman M T, Salaudin M, Maharjan P, et al. Natural wind-driven ultra-compact and highly efficient hybridized nanogenerator for self-sustained wireless environmental monitoring system. *Nano Energy*, 2019, 57: 256–268
- 3 Ju S, Ji C H. Impact-based piezoelectric vibration energy harvester. *Appl Energy*, 2018, 214: 139–151
- 4 Ghomian T, Mehraeen S. Survey of energy scavenging for wearable and implantable devices. *Energy*, 2019, 178: 33–49
- 5 Maharjan P, Toyabur R M, Park J Y. A human locomotion inspired hybrid nanogenerator for wrist-wearable electronic device and sensor applications. *Nano Energy*, 2018, 46: 383–395
- 6 Qian J, Jing X. Wind-driven hybridized triboelectric-electromagnetic nanogenerator and solar cell as a sustainable power unit for self-powered natural disaster monitoring sensor networks. *Nano Energy*, 2018, 52: 78–87

- 7 Fan K, Cai M, Liu H, et al. Capturing energy from ultra-low frequency vibrations and human motion through a monostable electromagnetic energy harvester. *Energy*, 2019, 169: 356–368
- 8 He J, Qian S, Niu X, et al. Piezoelectric-enhanced triboelectric nanogenerator fabric for biomechanical energy harvesting. *Nano Energy*, 2019, 64: 103933
- 9 Safaei M, Sodano H A, Anton S R. A review of energy harvesting using piezoelectric materials: state-of-the-art a decade later (2008–2018). *Smart Mater Struct*, 2019, 28: 113001
- 10 Chou X, Zhu J, Qian S, et al. All-in-one filler-elastomer-based high-performance stretchable piezoelectric nanogenerator for kinetic energy harvesting and self-powered motion monitoring. *Nano Energy*, 2018, 53: 550–558
- 11 Fan F R, Tian Z Q, Wang Z L. Flexible triboelectric generator. *Nano Energy*, 2012, 1: 328–334
- 12 Liang X, Jiang T, Liu G, et al. Triboelectric nanogenerator networks integrated with power management module for water wave energy harvesting. *Adv Funct Mater*, 2019, 29: 1807241
- 13 Xia K, Zhu Z, Fu J, et al. A triboelectric nanogenerator based on waste tea leaves and packaging bags for powering electronic office supplies and behavior monitoring. *Nano Energy*, 2019, 60: 61–71
- 14 Cheng P, Guo H, Wen Z, et al. Largely enhanced triboelectric nanogenerator for efficient harvesting of water wave energy by soft contacted structure. *Nano Energy*, 2019, 57: 432–439
- 15 Liu W, Xu L, Bu T, et al. Torus structured triboelectric nanogenerator array for water wave energy harvesting. *Nano Energy*, 2019, 58: 499–507
- 16 Qian J, He J, Qian S, et al. A nonmetallic stretchable nylon-modified high performance triboelectric nanogenerator for energy harvesting. *Adv Funct Mater*, 2020, 30: 1907414
- 17 Chandrasekhar A, Vivekananthan V, Kim S J. A fully packed spheroidal hybrid generator for water wave energy harvesting and self-powered position tracking. *Nano Energy*, 2020, 69: 104439
- 18 Huo H, Liu F, Luo Y, et al. Triboelectric nanogenerators for electro-assisted cell printing. *Nano Energy*, 2020, 67: 104150
- 19 Luo J, Wang Z, Xu L, et al. Flexible and durable wood-based triboelectric nanogenerators for self-powered sensing in athletic big data analytics. *Nat Commun*, 2019, 10: 5147
- 20 Tang W, Jiang T, Fan F R, et al. Liquid-metal electrode for high-performance triboelectric nanogenerator at an instantaneous energy conversion efficiency of 70.6%. *Adv Funct Mater*, 2015, 25: 3718–3725
- 21 Yang H, Pang Y, Bu T, et al. Triboelectric micromotors actuated by ultralow frequency mechanical stimuli. *Nat Commun*, 2019, 10: 2309
- 22 Yang X, Xu L, Lin P, et al. Macroscopic self-assembly network of encapsulated high-performance triboelectric nanogenerators for water wave energy harvesting. *Nano Energy*, 2019, 60: 404–412
- 23 Liu L, Tang W, Chen B, et al. A self-powered portable power bank based on a hybridized nanogenerator. *Adv Mater Technol*, 2018, 3: 1700209
- 24 Wang H, Zhu Q, Ding Z, et al. A fully-packaged ship-shaped hybrid nanogenerator for blue energy harvesting toward seawater self-desalination and self-powered positioning. *Nano Energy*, 2019, 57: 616–624
- 25 Wu Z, Guo H, Ding W, et al. A hybridized triboelectric-electromagnetic water wave energy harvester based on a magnetic sphere. *ACS Nano*, 2019, 13: 2349–2356
- 26 Huang T, Zhang Y, He P, et al. Energy harvesting: “self-matched” tribo/piezoelectric nanogenerators using vapor-induced phase-separated poly (vinylidene fluoride) and recombinant spider silk. *Adv Mater*, 2020, 32: 1907336
- 27 Rodrigues C, Gomes A, Ghosh A, et al. Power-generating footwear based on a triboelectric-electromagnetic-piezoelectric hybrid nanogenerator. *Nano Energy*, 2019, 62: 660–666
- 28 Su Y, Wen X, Zhu G, et al. Hybrid triboelectric nanogenerator for harvesting water wave energy and as a self-powered distress signal emitter. *Nano Energy*, 2014, 9: 186–195
- 29 Xiao T X, Liang X, Jiang T, et al. Spherical triboelectric nanogenerators based on spring-assisted multilayered structure for efficient water wave energy harvesting. *Adv Funct Mater*, 2018, 28: 1802634
- 30 Wang J, Pan L, Guo H, et al. Rational structure optimized hybrid nanogenerator for highly efficient water wave energy harvesting. *Adv Energy Mater*, 2019, 9: 1802892